Aerospace Science and Technology 100 (2020) 105826

Contents lists available at ScienceDirect

Aerospace Science and Technology

www.elsevier.com/locate/aescte

An intelligent cooperative mission planning scheme of UAV swarm in uncertain dynamic environment ☆

Ziyang Zhen *, Yan Chen, Liangdong Wen, Bing Han

College of Automation Engineering, Nanjing University of Aeronautics and Astronautics, Nanjing 211106, China

ARTICLE INFO

Article history:
Received 10 October 2019
Received in revised form 24 January 2020
Accepted 28 February 2020
Available online 6 March 2020
Communicated by Choon Ki Ahn

Keywords:
UAV swarm
Cooperative search-attack
Ant colony optimization
Artificial potential field
Mission planning

ABSTRACT

This paper presents an intelligent cooperative mission planning scheme for unmanned aerial vehicle (UAV) swarm, to search and attack the time-sensitive moving targets in uncertain dynamic environment, by using a hybrid artificial potential field and ant colony optimization (HAPF-ACO) method. In the search-attack mission environment of UAV swarm under the dynamic topology interaction, a time-sensitive target probability map is established. Based on the HAPF, the target attraction field, threat repulsive field and repulsive field are constructed for the environmental cognition. A distributed ACO algorithm is designed to improve the UAVs' global searching capability. For this mission planning problem, four time-sensitive moving target types and four constraint types of UAV swarm are considered, which will contribute to the practical applications of the HAPF-ACO. Several simulations are carried out to exhibit the superiority on the task execution efficiency and obstacle and collision avoidance performance of the proposed intelligent cooperative mission planning scheme.

1. Introduction

Unmanned aerial vehicle (UAV) has been increasingly employed to expand the abilities of the manned aerial vehicles in the modern air combat [1]. However, with the increasingly complex mission environment, the single UAV's mission execution capability is limited. Therefore, the cooperative control techniques of UAVs have been presented and widely investigated. The distribution, autonomy and robustness requirements of the cooperative control of UAV swarm are similar to the decentralized and self-organized characteristics of such biological groups as ant colony, bee colony, bird flock and fish school [2]. UAV swarm is an autonomous system inspired from the self-organized mechanism of biological groups, which largely improves the execution efficiency through complementary capabilities and coordinated operations.

Due to the large scale of UAV swarm, its computation and communication volume increase exponentially so that it is difficult to make decisions centrally within effective time. Therefore, the distributed decision-making schemes have been proposed for various applications, such as the swarm flocking [3], reconnaissance [4], surveillance [5], load transportation [6], search [7], task assignment and path planning [8–10]. For the search mission planning problem, the probability maps [11–14] and pheromone maps [15–17] have been widely employed. The target probability map can describe the dynamic target information in an unknown environment, based on which Ref. [14] used local information to model the target probability by considering the decentralized communication protocols. In addition, the pheromone map can increase the search efficiency by using the pheromone feedback mechanism to update the map in unknown environment. An improved pheromone map was designed for the UAV swarm collaborative search in limited area and time [17]. However, the collision avoidance among UAVs was commonly ignored, thus a hybrid scheme based on the virtual force and the receding horizon method was presented [18]. Besides, the bio-inspired optimizations have been widely applied in the mission planning of UAV warm. A pigeon-inspired algorithm was used in the multi-UAV cooperative search for the moving targets [19]. A bird swarm algorithm with a windowed edge potential function was designed for the target detection problem of leader-follower UAVs, the robustness of which was verified by the practical experiments [20]. The Markov decision process has been used in the surveillance mission planning of multiple UAVs [21], while the genetic algorithm

☆ This work was supported by the National Natural Science Foundation of China (Nos. 61973158, 61673209), and the Jiangsu Six Peak of Talents Program (No. KTHY-027).
* Corresponding author.
E-mail address: zhenziyang@nuaa.edu.cn (Z. Zhen).

https://doi.org/10.1016/j.ast.2020.105826
1270-9638/

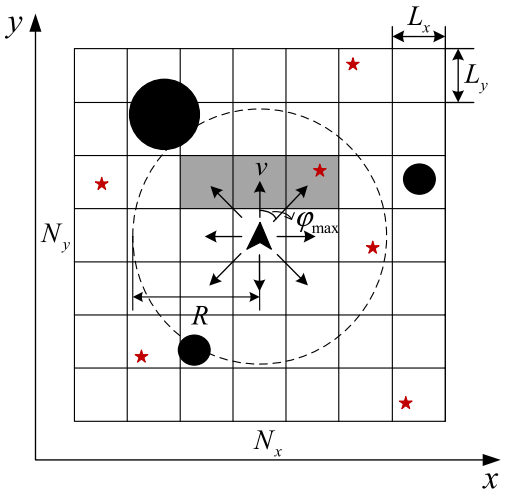

Fig. 1. Discrete mission area. (For interpretation of the colors in the figure(s), the reader is referred to the web version of this article.)

[22] and the ant colony optimization [23,24] have been used in the multi-UAV cooperative search-attack mission with stationary targets, especially, the collision avoidance and maximum range constraint of UAVs were considered in [24]. Furthermore, Ref. [25] addressed a coupled task allocation and path planning problem involving obstacles and no-fly zones for heterogeneous multiple UAVs, based on the Pythagorean hodograph curve. Above all, these bio-inspired algorithms commonly divide the global optimization problem into local optimization problems, which exhibits the effectiveness of the distributed cooperativity strategy.

In this paper, we aim to solve the cooperative search-attack mission planning problem of the fixed-wing UAV swarm in the unknown environment with time-sensitive moving targets. Different from the results in the literature, the main contributions are as follows: A hybrid artificial potential field and ant colony optimization (HAPF-ACO) algorithm is initially presented to search and attack the time-sensitive moving targets in an uncertain dynamic environment; The APF is constituted by target attraction field designed according to the target probability map (TPM), threat repulsive field designed based on the no-fly zone, and repulsive field among the UAV swarm; Four moving and time-sensitive target types are considered here, including unknown position, known position and unknown velocity, known position and unknown velocity direction, known position and velocity types; Not only the maneuverability constraints, collision avoidance constraints and obstacle avoidance constraints, but also the range constraints are considered in the mission planning problem.

The rest of this paper is organized as follows. In section 2, the UAV swarm cooperative search-attack mission planning problem is described. In section 3, the TPM, APF and pheromone map are designed, and the HAPF-ACO algorithm is proposed to realize the online search-attack decision making of UAV. In section 4, simulations are conducted to verify the effectiveness of the HAPF-ACO. Finally, a conclusion is given in section 5.

2. Modeling of cooperative mission planning problem for UAV swarm

In this section, the mission environment, dynamic topology interaction model and cooperative search-attack mission optimization model are established, respectively.

2.1. Mission environment model

It is assumed that the fixed-wing UAVs in the swarm are isomorphic, which namely each UAV has the same functional and performance constraints. Designating a task area $D \in R^2$, there are N_V UAVs in the swarm, N_T dynamic moving targets and N_p threats distributed. The mission of UAV swarm is to cooperatively search and attack the moving targets in the uncertain dynamic environment, through an efficient decision-making method.

Taking two-dimensional space as an example, as shown in Fig. 1, the mission area is discretized into a grid map with size of $N_x \times N_y$, and the length and width of each grid are recorded as L_x, L_y, respectively. The maneuver performance of the UAV is corresponding to the search of the discrete space, and the movement of the UAV is reflected as the motion in discrete grid points. The red five-pointed star represents the target, while the black circle represents the threat area, and the threat radius is R_t. The projection radius of the UAV's detection range on the plane of the mission area is assumed to be R. The targets and threats that appear in the detection range of the UAV can be detected by the UAV. Assume that the maximum turning angle of the UAV is $\varphi_{\max}$, the speed of the UAV is v, and the displacement in unit time is d, respectively. If the length and width of the grid are chosen as d, the gray grid indicates the possible position of the UAV at the next moment under the maneuver constraint.

2.2. Dynamic topology interaction model

Previous studies mostly assumed that UAV can interact with all individuals within its detection radius at the same time. This communication method will cause the number of UAV's communication neighbors to change greatly with the density of the swarm distribution, which would have a greater impact on traffic. Here, a dynamic topology interaction model is designed by simulating the information interaction mechanism of the biological swarm. This model keeps the number of neighbors of the UAV basically constant. The advantages are especially obvious when the swarm size is large and the distribution is dense, which can greatly reduce the traffic of the swarm.

To reflect this topological interaction feature, the cooperative radius r_i^{coor} is defined to represent the actual interaction scale of the individual. The UAV can sense the state information of the individual within its cooperative radius in real time, and its interactive neighbor set can be expressed as

$$N_i^c = \left\{ j \,|\, \|x_i - x_j\| \le r_i^{coor},\ j \in \{1, 2, \cdots, N_V\},\ j \ne i \right\} \tag{1}$$

Since the location of the UAV changes in real time, in order to achieve a substantially constant number of neighbors, the cooperative radius r_i^{coor} is dynamically adjusted by

$$\dot{r}_i^{coor} = k \cdot R_{sen} \cdot \left(1 - \left|N_i^c\right| / n_{topo}\right) \tag{2}$$

where $0 < k < 1$ is the adjusting rate. R_{sen} is the perceived radius of the UAV, which is the upper bound of the communicate distance, i.e., $r_i^{coor} \le R_{sen}$. $|N_i^c|$ is the current number of neighbors of the i-th UAV. n_{topo} is the expected number of neighbors.

The communication network structure between the UAVs can be represented by the graph $G(V, E, A)$, where $V = \{V_i, i = 1, 2, \cdots, N_V\}$ are N_V UAV nodes of the graph G. V_i represents the i-th UAV. $E \in V \times V$ represents the edge set of the graph G. Each edge $e_{ij} = (v_i, v_j) \in E$ indicates that the j-th UAV can send information to the i-th UAV, and v_j is called the parent node of v_i. The set of all parent nodes of v_i is the neighbor set of v_i. The relationship of each node in the graph is represented by an adjacency matrix $A = [a_{ij}] \in R^{n \times n}$, where a_{ij} represents the connection weight of node v_j to v_i, expressed by

$$a_{ij} = \begin{cases} 1, & d_{ij} \le r_i^{coor} \\ 0, & d_{ij} > r_i^{coor} \end{cases} \tag{3}$$

where d_{ij} is the distance between the i-th UAV and the j-th UAV.

2.3. Cooperative search-attack mission optimization model

The purpose of cooperative search-attack of UAV swarm is to cover the mission area, find and destroy more targets under the given constraints. Therefore, the target attack benefit J_T and environmental search benefit J_E are the performance indicators of the cooperative search-attack mission, J_T is the total value of the targets which have been attacked, J_E can be expressed by the coverage rate of the mission area, calculated as the ratio of grids which have been searched to all the grids in mission area, respectively defined as

$$\begin{cases} J_T(k) = \sum\limits_{m=1}^{N_{\text{target}}(k)} value_m \\ J_E(k) = \sum\limits_{m=1}^{N_x} \sum\limits_{n=1}^{N_y} grid_{(m,n)}(k) \Big/ (N_x \times N_y) \end{cases} \tag{4}$$

where $N_{\text{target}}(k)$ is the total number of targets attacked at time k, $value_m$ is the value of the m-th target, respectively. $grid_{(m,n)}(k) = 0$ if the grid (m, n) is not covered at time k, otherwise, $grid_{(m,n)}(k) = 1$.

The goal of the UAV swarm's cooperative search-attack mission is to obtain the decision input to maximize the overall performance index under certain constraints. Therefore, the cooperative search-attack mission optimization model is constructed as

$$\begin{aligned} &U^*(k) = \arg\max_{U(k)} \left(\omega \times J_T(k) + (1 - \omega) \times J_E(k)\right) \\ &\text{s.t.} \\ &\begin{cases} C_m : \Delta\varphi_i(k) - \varphi_{\max} \le 0 & (i = 1, 2, \cdots, N_V) \\ C_c : d_{\min} - d_{ij}(k) \le 0 & (i, j = 1, 2, \cdots, N_V;\ i \ne j) \\ C_t : R_l^T - d_{il}^T(k) \le 0 & (i = 1, 2, \cdots, N_V;\ l = 1, 2, \cdots, N_p) \\ C_r : L_{past}^i(k) - L_{\max}^i \le 0 & (i = 1, 2, \cdots, N_v) \end{cases} \end{aligned} \tag{5}$$

where $\omega \in \{0, 1\}$, $\omega = 1$ indicates that the execution of an attack mission, while $\omega = 0$ indicates that a search mission is performed. U^* is the optimal decision input obtained for the solution which represents the position of the UAV at the next moment. C_m, C_c, C_t and C_r represent the UAV's maneuver constraints, collision avoidance constraints, obstacle avoidance constraints and range constraints, respectively. $d_{ij}(k)$ is the distance between the i-th UAV and j-th UAV, which should be greater than the minimum safe distance $d_{\min}$ to prevent collisions between UAVs. $d_{il}^T(k)$ is the distance between the i-th UAV and the l-th threat, which should be greater than the radius of the threat R_l^T to avoid obstacles. $L_{past}^i(k)$ is the traversed distance of the i-th UAV, which should be less than the i-th UAV's maximum range $L_{\max}^i$, to prevent fuel exhaustion during flight.

Considering that the UAV swarm is a non-central distributed system, the UAV swarm's global performance indicators (4) are decomposed into the local performance indicators of a single UAV, thus

$$\begin{cases} J_T = \sum\limits_{i=1}^{N_V} \mu_i J_{Ti} \\ J_E = \sum\limits_{i=1}^{N_V} \mu_i J_{Ei} \end{cases} \tag{6}$$

where μ_i represents the weight of the i-th UAV. Then a distributed optimization model is designed as

$$\begin{aligned} &U_i^*(k) = \arg\max_{U_i(k)} \left(\omega \times J_{Ti}(X_i, \tilde{X}_i) + (1-\omega) \times J_{Ei}(X_i, \tilde{X}_i)\right) \\ &\tilde{X}_i = \left\{X_j \mid j \in N_i^c\right\} \\ &\text{s.t.} \quad C_i \leq 0 \quad i = 1, 2, \cdots, N_v \end{aligned} \tag{7}$$

where X_i and $\tilde{X}_i$ are the state of the i-th UAV and its neighbors, respectively. $J_{Ti}(X_i, \tilde{X}_i)$ is i-th UAV's the target attack benefit, $J_{Ei}(X_i, \tilde{X}_i))$ is i-th UAV's environmental search benefit, C_i is a set of constraints.

3. Design of HAPF-ACO algorithm

In this section, the HAPF-ACO algorithm is proposed for the cooperative search-attack mission planning, including the designs of target probability map, environmental cognition, pheromone update mechanism and state transition rule.

3.1. Target probability map

The TPM describes the distribution of the targets in the mission area, aiming to improve the possibility of finding the targets. In the discretized mission area, $p_{mn}^i(k)$ is the target existence probability of the grid (m, n) learned by the i-th UAV, and $p_{mn}^i(k) \in [0, 1]$. The target existence probability of all the grids in the mission area D constitutes a probability distribution matrix

$$\mathrm{TPM}_i(k) = \left\{p_{mn}^i(k) \mid m = 1, 2, \cdots, N_x,\ n = 1, 2, \cdots, N_y\right\} \tag{8}$$

3.1.1. TPM initialization

At the initial moment, each UAV initializes its own TMP according to the priori information of the targets including the initial positions, speeds and movement directions. Considering the time-sensitive targets, they can be divided into the following four types.

a) When the initial positions of the targets are unknown, the probabilities of the targets in any grid in the mission area are the same, and the uniform distribution can be used to describe the target probability distribution density function

$$f(x, y) = \frac{1}{N_x \cdot N_y \cdot L_x \cdot L_y}, \quad (x, y) \in D \tag{9}$$

where $f(x, y)$ indicates the target existence probability at the location (x, y).

b) When the initial position of the target is known as (x_*, y_*), the target speed is unknown. Considering the possible error of prior information, the existence probability at the actual position (x_0, y_0) of the target can be considered to obey the two-dimensional normal distribution $N(x_*, y_*, \sigma_0^2, \sigma_0^2, \rho)$. Because x_0, y_0 are independent of each other, $\rho = 0$, thus

$$f_0(x_0, y_0) = \frac{1}{2\pi\delta_0^2} \mathrm{e}^{-\left(\frac{(x_0 - x_*)^2}{2\delta_0^2} + \frac{(y_0 - y_*)^2}{2\delta_0^2}\right)} \tag{10}$$

where $\delta_0^2 \geq 0$ is the normal distribution variance, which reflects the accuracy of the prior information. After time t_0, the UAV reaches the mission area and begins to perform the mission. Due to the time-sensitive nature of the target, the target's position changes from the UAV receives the command to the UAV reaches the mission area. The motion information of the target is unknown, and is an independent incremental process. It is reasonable to describe the randomness of the target motion by using the Wiener random process. $X(t) \sim \mathrm{N}(0, \delta_e^2 t_0)$, $\mathrm{Y}(t) \sim \mathrm{N}(0, \delta_e^2 t_0)$, and the target probability distribution density function is expressed as

$$f(x, y) = \frac{1}{2\pi(\delta_0^2 + \delta_e^2 t_0)} \mathrm{e}^{-\left(\frac{(x - x_*)^2}{2(\delta_0^2 + \delta_e^2 t_0)} + \frac{(y - y_*)^2}{2(\delta_0^2 + \delta_e^2 t_0)}\right)} \tag{11}$$

where δ_e is constant and represents the Wiener random process variance.

c) When the initial position of the target is known as (x_*, y_*), the target initial speed is v, the target motion direction is unknown, the target actual position (x_0, y_0) is a random variable, and the UAV enters the mission area after time t_0. Since the target speed is fixed, it is equivalent to the target probability density has shifted, and the probability density $f(x, y)$ at the point (x, y) is transferred from the arc with radius vt_0 and the center of the circle (x, y), given by

$$f(x, y) = \frac{1}{2\pi v t_0} \int_L f_0(x_0, y_0) \mathrm{d}s \tag{12}$$

where L is a circle with radius vt_0 and the center (x, y). The probability of transition is $\frac{1}{2\pi v t_0}$. After transforming with first form curvilinear integral, it is transformed into

$$f(x, y) = \frac{1}{(2\pi\delta_0)^2} \int_{\theta=0}^{2\pi} \mathrm{e}^{-\left(\frac{(x + vt_0 \cdot \cos\theta - x_*)^2}{2\delta_0^2} + \frac{(y + vt_0 \cdot \sin\theta - y_*)^2}{2\delta_0^2}\right)} \mathrm{d}\theta \tag{13}$$

d) If the initial position of the target is known as (x_*, y_*), the target motion velocity is v, the motion direction is θ, $\theta \in [0, 2\pi]$, the distribution of the target position is offset from the actual position (x_0, y_0), and the offset is $(vt_0\cos(\theta), vt_0\sin(\theta))$. Then the probability density function is

$$f(x, y) = \frac{1}{2\pi\delta_0^2} e^{-\left(\frac{(x-vt_0\cos(\theta)-x_*)^2}{2\delta_0^2} + \frac{(y-vt_0\sin(\theta)-y_*)^2}{2\delta_0^2}\right)} \tag{14}$$

Then the target existence probability p_{mn}^i of a single grid (m, n) can be expressed as

$$p_{mn}^i = \int_{(n-1)L_y}^{nL_y} \int_{(m-1)L_x}^{mL_x} f(x, y)dxdy \tag{15}$$

And the normalization is performed to obtain the initial target probability distribution matrix

$$\mathrm{TPM}_i(m, n) = p_{mn}^i / \sum_{m=1}^{N_x} \sum_{n=1}^{N_y} p_{mn}^i \tag{16}$$

3.1.2. Probe update

As the search-attack mission progresses, the UAV's awareness of the area is deepened. Therefore, in each decision cycle, each UAV needs to dynamically update the TMP based on the sensor detection information. The target detection probability related with the sensor detection distance is given by

$$p(b_k = 1|d_k) = \begin{cases} P_D & d_k \le d_{in} \\ P_D - \dfrac{(P_D - P_F)(d_k - d_{in})}{(d_{out} - d_{in})} & d_{in} < d_k \le d_{out} \\ P_F & d_k > d_{out} \end{cases} \tag{17}$$

where $b_k \in \{0, 1\}$ is the detection result, $b_k = 0$ indicates that there is no target in the sensor field of view (FOV), $b_k = 1$ indicates that there is a target, $P_D \in [0, 1]$ is the probability of detection for the sensor, $P_F \in [0, 1]$ is the false alarm probability. d_k indicates the distance from the sensor to the target, if $d_k < d_{in}$, the sensor can detect the target, but because of the uncertainty of the observation, the probability of detecting the target is P_D, if $d_k > d_{out}$, the sensor cannot detect the target, if the target is still reported detected, it is false alarm, the probability of detection is P_F.

Ref. [26] considers a sensor that covers more than one grid and updates the target existence probability map according to the sensor detection results. Here we assume that there is only one cell in the FOV, then a simplified target existence probability map update formula based on Bayesian probability formula is designed as

$$p_{mn}^i(k+1) = \begin{cases} \tau\, p_{mn}^i(k) & \text{(not detected)} \\ \dfrac{P_D \cdot p_{mn}^i(k)}{P_F + (P_D - P_F) \cdot p_{mn}^i(k)} & \big(\text{detected and } b(k) = 1\big) \\ \dfrac{(1 - P_D) \cdot p_{mn}^i(k)}{1 - P_F + (P_F - P_D) \cdot p_{mn}^i(k)} & \big(\text{detected and } b(k) = 0\big) \end{cases} \tag{18}$$

where $\tau \in [0, 1]$ is the attenuation coefficient and is used to characterize the dynamic environment.

3.1.3. Forecast update

The time interval between the two decisions is Δt. In order to ensure the accuracy of the probability map and improve the search-attack efficiency of the UAV swarm, the motion of the UAV is predicted and the corresponding TPM is updated.

The position of the target of the k-th decision cycle is a random variable (x^k, y^k), and the k-th periodic probability density function is $f_k(x^k, y^k)$, expressed by the full probability formula

$$f_k\big(x^k, y^k\big) = \iint f\big((x^k, y^k)|(x^{k-1}, y^{k-1})\big) f_{k-1}\big(x^{k-1}, y^{k-1}\big) dx^{k-1} dy^{k-1} \tag{19}$$

According to the different target motion information, the conditional probability can be divided into the following three types.

a) The magnitude and direction of the velocity are unknown. The motion of the target during the period from (k-1)-th periodic to k-th periodic is an independent incremental process, $X(t) \sim \mathrm{N}(0, \delta_e^2 \Delta t)$ and $\mathrm{Y}(t) \sim \mathrm{N}(0, \delta_e^2 \Delta t)$ are estimated by the Wiener random process. The conditional probability density is

$$f_k\big((x^k, y^k)|(x^{k-1}, y^{k-1})\big) = \frac{1}{2\pi\delta_e^2\Delta t} \mathrm{e}^{-\left(\frac{(x^k - x^{k-1})^2}{2\delta_e^2\Delta t} + \frac{(y^k - y^{k-1})^2}{2\delta_e^2\Delta t}\right)} \tag{20}$$

b) The magnitude of the velocity is known and direction of the velocity is unknown. After a period of time, the target is evenly distributed on the arc with radius $v\Delta t$ and the center of the circle (x^{k-1}, y^{k-1}). The conditional probability density is expressed as

$$f_k\left(\left(x^k, y^k\right)|\left(x^{k-1}, y^{k-1}\right)\right) = \begin{cases} \dfrac{1}{2\pi v \Delta t} & (x-x_0)^2 + (y-y_0)^2 = (v\Delta t)^2 \\ 0 \quad \text{other} \end{cases} \tag{21}$$

c) The magnitude and direction of the velocity are known. The distribution of the target position is offset from the position of the previous cycle. The offset is $(v\Delta t \cdot \cos\theta, v\Delta t \cdot \sin\theta)$. The conditional probability density function is expressed as

$$f_k\left(\left(x^k, y^k\right)|\left(x^{k-1}, y^{k-1}\right)\right) = \begin{cases} 1 & x^k = x^{k-1} + v \cdot \cos\theta, \quad y^k = y^{k-1} + v \cdot \sin\theta \\ 0 & \text{other} \end{cases} \tag{22}$$

Similar to the TPM initialization, the predicted updated TPM will be obtained after normalization, and the result is used as the priori information for the next moment decision.

3.2. Environmental cognition based on APF

The UAV's motion environment is abstracted into a potential field, in which the target produces attraction force on the UAV and the obstacle generates repulsive force on the UAV. The combined attraction force and repulsive force are used to control the movement of the UAV, guide the UAV to a specified target position and effectively avoid the environmental threats. Considering the collision avoidance problem between UAVs, the potential field between UAVs is also introduced.

3.2.1. Target attraction field

Based on the APF method, the target will generate a gravitational field $U_{att}(X)$ and the UAV is driven close to the target by applying attraction force F_{att} to the UAV. In the search-attack mission of the UAV swarm, the greater the target existence probability is, the more the UAV tends to transfer to the grid. Then, the TPM is used as the target attraction field.

According to the real-time TPM_i of the i-th UAV, the attraction field is designed as

$$U_{att,i} = k_{att} \cdot \text{TPM}_i \tag{23}$$

where $k_{att} > 0$ is the gravitational coefficient. The target attraction force is the gradient of the target attraction field at the location of the UAV:

$$F_{\text{att},i}(X_i) = \nabla U_{\text{att},i}(X_i) \tag{24}$$

The UAV will move toward the fastest rising direction of the target existence probability, under the action of the target attraction force. When it is confirmed that the target is detected, the UAV will approach the target according to the target attraction force, until the target is within the attack radius of the UAV, and then attack the target. If multiple targets are found at the same time, the target with higher value is preferentially selected to attack.

3.2.2. Threat repulsive field

The UAV may encounter the no-fly zone caused by local bad weather, terrain blocking and enemy threats. In order to ensure the safety of the UAV and the smooth execution of the task, the UAV needs to avoid the threat areas. Based on the artificial potential field method, the threat area generates a repulsive field U_{rep}^T which can drive the UAV away from the threat by applying a repulsive force.

Suppose that the threat area is circular, its center position is X_t, and the radius is R_t. The UAV can detect the threat when the distance from the UAV to the edge of the threat zone is less than the UAV's detection radius R, that is, the distance between the UAV and the threat zone center is less than $R + R_t$. To strictly prevent the UAV from entering the threat zone, the designed repulsive force should increase as the distance between the UAV and the threat decreases. If the position of the i-th UAV is X_i, then the threat repulsion is designed as

$$F_{rep,i}^T(X_i) = \begin{cases} k_{rep} \cdot \sum\limits_{l \in S_i} \left(\dfrac{1}{\|x_{il}\|^2} - \dfrac{1}{(d_{\max,l}^t - d_0)^2} \right) \cdot \hat{x}_{il}, & \|x_{il}\| \le d_{\max,l}^t \\ 0, & \|x_{il}\| > d_{\max,l}^t \end{cases} \tag{25}$$

where k_{rep} is the repulsion coefficient, $x_{il} = X_i - X_t^l$ is the position vector of the detected l-th threat pointing to the i-th UAV, $\hat{x}_{il} = x_{il}/\|x_{il}\|$. $d_{\max,l}^t$ is the radius of action of the l-th threat repulsion field, if the distance between the UAV and the threat center is larger than $d_{\max,l}^t$, the UAV is no longer subject to repulsive force; $d_0 \ge R_t$ is the minimum safe distance, the distance between the UAV and the threat center must not be less than d_0.

3.2.3. Repulsive field between the UAVs

When the UAV swarm collaboratively executes missions, with the increase of the number of UAVs in the same task airspace, there must be some UAVs' search routes that overlap in time and space, resulting in collisions between UAVs. In order to ensure the security of the UAV, the neighboring UAVs with too close distances will generate repulsive fields U_{rep}^V to achieve dynamic collision avoidance coordination between the UAV swarm. This paper builds the repulsive field between the UAVs based on the following generalized Morse function

$$U_{rep,i}^V = \begin{cases} \sum\limits_{j \in N_i^c} \dfrac{b}{e^{\frac{\|x_{ij}\|}{c}} - e^{\frac{\|x_{ij}\|_{\min}}{c}}}, & \|x_{ij}\| \in \left[d_{\min}, d_{\max}^v\right] \\ 0, & \|x_{ij}\| \notin \left[d_{\min}, d_{\max}^v\right] \end{cases} \tag{26}$$

where b and c are adjustable parameters, which determines the magnitude and rate of change of the repulsive field, respectively. $x_{ij} = X_i - X_j$ is the position vector from the j-th UAV to the i-th UAV. $[d_{\min}, d^v_{\max}]$ is the range of the repulsive field between the UAVs, $d_{\min}$ is the minimum safe distance between the UAVs. If $\|x_{ij}\| < d_{\min}$, the collision occurs between the UAVs. $d^v_{\max}$ is the maximum operating distance of the repulsive field between the UAVs.

As the negative gradient of the repulsive field, the repulsion between the UAVs is

$$F^V_{rep,i}(X_i) = -\nabla U^V_{rep,i}(X_i) = \sum_{j \in N_i^c} \frac{b}{c} \cdot \frac{1}{(e^{\frac{\|x_{ij}\|}{c}} - e^{\frac{\|x_{ij}\|_{\min}}{c}})^2} e^{\frac{\|x_{ij}\|}{c}} \cdot \hat{x}_{ij} \tag{27}$$

where $\hat{x}_{ij} = x_{ij}/\|x_{ij}\|$ is the unit vector pointing from the j-th UAV to the i-th UAV. When the parameters b and c are determined, the magnitude of the repulsion between the UAVs depends only on the distance. The closer the distance is, the greater the repulsive force is, which can effectively achieve anti-collision between the UAVs.

3.3. Pheromone update mechanism

In order to achieve task cooperation among the UAVs, pheromone values are assigned to all grids of the mission area. A pheromone update mechanism is designed to avoid the UAV searching the grids that have been searched by other UAVs, and drive them to search for grids that haven't been searched.

3.3.1. Distributed pheromone structure

The pheromone concentration of different grids reflects the degree of attraction of the grid to the UAV. The higher the pheromone concentration, the more the UAV tends to transfer to the grid. Therefore, the UAV can reasonably update the local pheromone structure according to the search situation, and can realize the task coordination of the swarm.

The UAV swarm adopts a distributed architecture without a central node. Therefore, there is no public pheromone in the swarm. Each UAV establishes its local pheromone structure and only updates the pheromone structure maintained by itself. The pheromone concentration values of all grids in the mission area at a certain time constitute the local pheromone structure of the UAV at that moment, indicating the UAV's perception of the current environmental search situation. The local pheromone structure $\tau^i(k)$ maintained by the i-th UAV is

$$\tau^i(k) = \left\{\tau^i_{(x,y)}(k)\right\}, \quad x = 1, \cdots, N_x, \quad y = 1, \cdots, N_y \tag{28}$$

where $\tau^i_{(x,y)}(k)$ represents the pheromone concentration value at the grid (x, y).

At the same time, in order to prevent the pheromone concentration in a certain area from being too high or too low, the lower limit $\tau_{\min}$ and upper limit $\tau_{\max}$ of the pheromone concentration value are set, and the pheromone concentration of all the grids should be within the range $[\tau_{\min}, \tau_{\max}]$, that is, the pheromone structure maintained by any UAVs satisfies

$$\tau^i_{(x,y)}{}'(k) = \begin{cases} \tau_{\min}, & \tau^i_{(x,y)}(k) < \tau_{\min} \\ \tau^i_{(x,y)}(k), & \tau_{\min} \le \tau^i_{(x,y)}(k) \le \tau_{\max} \\ \tau_{\max}, & \tau^i_{(x,y)}(k) > \tau_{\max} \end{cases} \tag{29}$$

3.3.2. Local pheromone update mechanism

In order to avoid excessive search of a certain area by the swarm, a coordination mechanism should be established between the UAVs. Therefore, local pheromone update rules are designed to ensure regional search coordination between UAVs. After the UAV completes the one-step search, it updates the maintained local pheromone according to the current state information of itself and neighbor UAVs, to reduce the pheromone concentration of the searched grid, and prevents the swarm from repeatedly searching for a certain area.

The state information of the entire swarm that the i-th UAV masters at time k is

$$\begin{cases} Info_i(k) = \left\{Info_{j,i}(k_{j,i}), V_j \in V\right\} \\ Info_{j,i}(k_{j,i}) = \left\{x_{j,i}(k_{j,i}), y_{j,i}(k_{j,i}), \psi_{j,i}(k_{j,i})\right\} \end{cases}, \quad k_{j,i} \le k \tag{30}$$

where $Info_{j,i}(k_{j,i})$ is the historical state information of the j-th UAV obtained by the i-th UAV at time k, including location information $x_{j,i}(k_{j,i})$, $y_{j,i}(k_{j,i})$ and motion direction information $\psi_{j,i}(k_{j,i})$. According to this, the i-th UAV predicts the state of the swarm at time k

$$\begin{cases} Info^*_i(k) = \left\{Info^*_{j,i}(k), V_j \in V\right\} \\ Info^*_{j,i}(k) = \left\{x^*_{j,i}(k), y^*_{j,i}(k), \psi^*_{j,i}(k)\right\} \end{cases} \tag{31}$$

Based on the prediction information, the i-th UAV updates the local pheromone structure according to the following update mechanism

$$\begin{cases} \tau^i_{(x,y)}(k+1) = \tau^i_{(x,y)}(k) - \Delta\tau^i_{l(x,y)}(k) \\ \Delta\tau^i_{l(x,y)}(k) = \sum_{j \in N_i^c} \Delta\tau^{(i,j)}_{l(x,y)}(k) \end{cases} \tag{32}$$

$$\Delta\tau_{l(x,y)}^{(i,j)}(k)=\begin{cases}\Delta\tau_{l_0}\times\dfrac{R^4-d^4((x,y),(x_{j,i}^*(k),y_{j,i}^*(k)))}{R^4}, & d\big((x,y),\big(x_{j,i}^*(k),y_{j,i}^*(k)\big)\big)\le R\\ 0, & d\big((x,y),\big(x_{j,i}^*(k),y_{j,i}^*(k)\big)\big)>R\end{cases}\tag{33}$$

where $\Delta\tau_{l(x,y)}^{(i,j)}(k)$ is the pheromone attenuation caused by the j-th neighboring UAV on the grid (x,y), $\Delta\tau_{l_0}$ is the local pheromone attenuation constant, $d((x,y),(x_{j,i}^*(k),y_{j,i}^*(k)))$ is the distance between the grid (x,y) and the grid $(x_{j,i}^*(k),y_{j,i}^*(k))$.

3.3.3. Global pheromone update mechanism

A new target may appear in the area that has been searched, which leads to increased uncertainty and the degree of attraction to the UAV. Therefore, it is necessary to correspondingly enhance the pheromone concentration of each grid.

A global pheromone update mechanism is designed to perform a pheromone enhancement operation on all grids at regular intervals:

$$\tau_{(x,y)}^{i}(k+1)=\tau_{(x,y)}^{i}(k)+F\times\Delta\tau_{g_0}\tag{34}$$

where $F\in(0,1)$ is environmental uncertainty factor and $\Delta\tau_{g_0}$ is update step. The stronger dynamic the environment is, the larger F is, and the more pheromone concentration increases.

3.4. State transition rule

The task area is discretized, and then the local artificial potential field and pheromone structure information are initialized. After that, the algorithm chose deterministic state transition or a probabilistic state transition according to the criterion. When the ant colony enters the next node, the state information is updated, and the target probability map is predicted until the end of the target point is reached.

3.4.1. Deterministic transition rule

Assuming the current grid is s_i, considering the range constraint of the UAV, the deterministic transition rules are designed as

$$s_j=\omega_1\times\arg\min_{j\in\Omega}\{\theta_j\}+\omega_2\times\arg\min_{j\in\Omega}\big(\big|L_{\max}-L_{past}(k+1)-D_{left}(k+1)\big|\big),\quad q<\lambda F/F_{\max}\tag{35}$$

where Ω is the candidate grid set of the ant at the next time. θ_j is the angle between the path from the current grid to the candidate grid s_j and the direction of the current grid potential field force, $L_{\max}$ is the maximum range, $L_{past}(k+1)$ is the traversed distance of the UAV at the next moment, $D_{left}(k+1)$ is the distance between the starting position or the specific destination and the grid s_j, the sum of ω_1 and ω_2 is 1, if the traversed distance of the UAV at time $k+1$ is less than or equal to half of the maximum range, ω_2 is 0, otherwise ω_2 is 1, q is the random number in the range $[0,1]$, λ represents the environmental perception factor, F represents the magnitude of the potential field force of the current grid, $F_{\max}$ represents the maximum value of the potential field force in the current detection range. When F is large, that is, there are targets, threats or ants that are too close nearby, deterministic transfer will be performed.

Select a grid with the smallest angle with the current potential field direction from the candidate grid as the transfer node at the next moment, so that the ant can quickly approach the target, away from the threat area or the ants that are too close under the action of the potential field force.

3.4.2. Heuristic transition rules

When $q\ge\lambda F/F_{\max}$, heuristic transition rule is adopted. When performing state transition, the UAV current position $p(k)$, heading $\varphi(k)$, maximum turning angle $\varphi_{\max}$, and displacement per unit decision time Δd should be considered to obtain the candidate grid of the ant at the next time. Then the transfer grid of the ant at the next moment is selected based on the pheromone concentration and heuristic information of each candidate grid. The state transition probability $p_{ij}(k)$ of the ant moving from the current grid s_i to the candidate grid s_j is defined as

$$p_{ij}(k)=\begin{cases}\dfrac{[\tau_{ij}(k)]^{\alpha}\times[\eta_{ij}(k)]^{\beta}}{\sum_{s_j\in\Omega}[\tau_{ij}(k)]^{\alpha}\times[\eta_{ij}(k)]^{\beta}}, & s_j\in\Omega\\ 0, & s_j\notin\Omega\end{cases}\tag{36}$$

where $\tau_{ij}(k)$, $\eta_{ij}(k)$ are the pheromone concentration and heuristic information from the grid s_i to s_j, respectively. α is the information heuristic factor, β is the expectation heuristic factor. The larger $p_{ij}(k)$ is, the greater the probability that the ant move to the candidate grid s_j is.

Based on the state transition probability of each candidate grid obtained by (36), and considering the range constraint of the UAV, the heuristic state transition rules are designed as

$$s_j=\begin{cases}\omega_1\times\arg\max_{j\in\Omega}\{[\tau_{ij}^{\alpha}]\times[\eta_{ij}^{\beta}]\}+\omega_2\times\arg\min_{j\in\Omega}\big(\big|L_{\max}-L_{past}(k+1)-D_{left}(k+1)\big|\big), & q_1\le q_0\\ S, & \text{other}\end{cases}\tag{37}$$

where q_1 is the random number in the range $[0,1]$, $0<q_0<1$. S is a random variable selected according to (36). The ant tends to choose a grid with larger pheromone concentration and heuristic information. By designing the coverage of the mission area as heuristic information, the ants move to unsearched grids with higher probability, which increases the possibility of finding targets.

Table 1
Target movement information.

Target label	Coordinate (km)	Speed (m/s)	Moving direction	Value
1	(80,70)	unknown	unknown	3
2	(15,60)	unknown	unknown	3
3	(45,50)	unknown	unknown	2
4	(70,20)	unknown	unknown	4
5	(30,40)	30	unknown	3
6	(15,90)	20	unknown	1
7	(40,10)	40	unknown	3
8	(85,30)	50	unknown	5
9	(8,15)	10	1	2
10	(55,20)	20	1.7	3
11	(60,85)	25	4	4
12	(25,70)	30	5	3
13	(65,60)	0	0	1
14	(20,30)	0	0	2
15	(40,80)	0	0	1
16	(75,40)	0	0	2

Table 2
Description and value of the HAPF-ACO algorithm parameters.

Parameter name	Parameter value	Parameter description
$\Delta\tau_{l_0}$	0.1	Attenuation constant of local pheromone
$\Delta\tau_{g_0}$	15	Update constant of global pheromone
F	0.02	Environmental uncertainty factor
α	1	Importance factor of pheromone concentration in state transition
β	3	Importance factor of heuristic function in state transition
N_t	10	Iteration number threshold

Further, when the ant is surrounded by the searched grids, the heuristic information of the candidate grids is basically the same, which results in that the ant may not or takes a long time to jump out of the local search. Therefore, an improved transfer rule is used: if the coverage rate keeps no change for certain iterations N_t, then the ant will move to the nearest unsearched grid. It will increase the coverage rate of the mission area and improve the global search ability.

3.5. Flow chart of HAPF-ACO

Based on the above design, the flow of the adopted HAPF-ACO algorithm is shown in Fig. 2. The traditional heuristic ACO algorithm only considers the influence of pheromone concentration and heuristic information on ant state transition. In the HAPF-ACO algorithm, the APF is introduced into the heuristic ACO algorithm, given by (9)–(27). In addition to the influence of pheromone concentration given by (30)–(34) and heuristic information, the effect of APF force should be considered in the state transition of ants, so as to realize online obstacle avoidance and collision avoidance. Therefore, the HAPF-ACO algorithm improves the ant's state transition rules, combines the deterministic transition given by (35) and heuristic transition given by (37) according to the ant's grid potential force, and adds UAV flight constraints to the state transition rules.

4. Simulation analysis

In order to verify the superiority of the HAPF-ACO algorithm for the search-attack problem of UAV swarm, the MATLAB based simulations are carried out.

4.1. Mission scenarios and parameter settings

The mission area is 100 km × 100 km and is discretized to 100 × 100 grids. There are 16 targets distributed in the area, and each type has 4 targets. The target motion state is randomly generated using the corresponding probability distribution, the initial position variance $\delta_0 = 5$ and the Wiener random process parameter $\delta_e = 2$. The target movement information is shown in Table 1, where the targets 13-16 are evenly distributed unknown targets. Assume that the UAVs enter the mission area after $t_0 = 50$ s from receiving the task command and the speed is 100 m/s. Each decision step is 10 s, that is, the UAV moves one grid per decision. The UAV's maximum turning angle $\varphi_{\max} = 45°$, the detection radius is 3 km, the attack radius is 1 km, the sensor detection probability $P_D = 0.9$, and the false alarm probability $P_F = 0.1$. The other relevant parameters in the HAPF-ACO algorithm are shown in Table 2.

4.2. Task execution efficiency analysis

Assuming that two UAVs perform the missions, the initial positions are at $(10, 10)$ km and $(90, 90)$ km without considering the threat in the mission area. The expected number of neighbors $n_{topo} = 1$, the perceived radius of the UAV is 50 km. The following three algorithms are investigated:

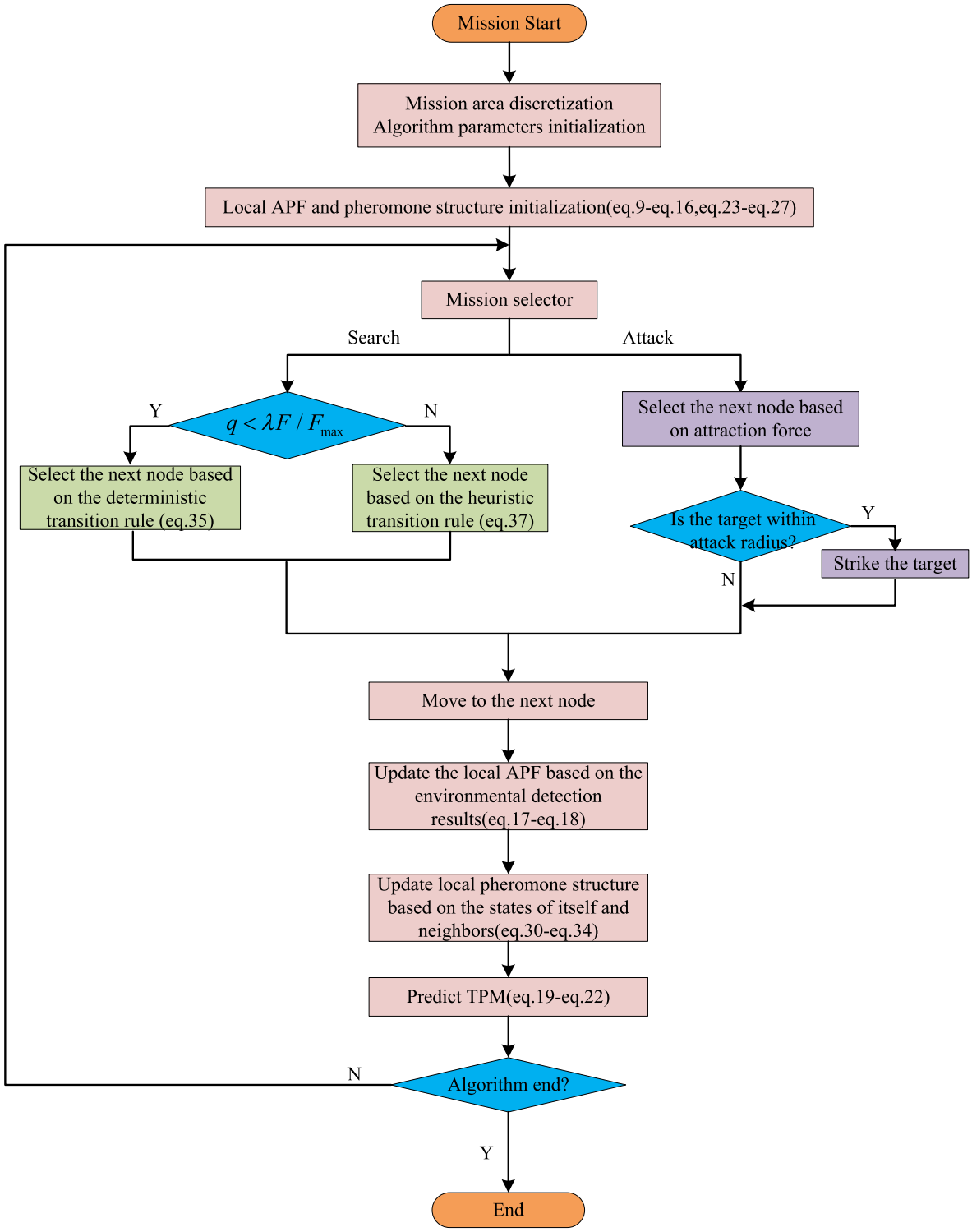

Fig. 2. Flow chart of HAPF-ACO algorithm.

Algorithm 1. Particle swarm optimization (PSO) is a popular bionic intelligent optimization algorithm which has been applied in the mission planning problem [4]. Here, the PSO algorithm is used to solve this search-attack problem, to be compared with the proposed algorithm.

Algorithm 2. An ant colony optimization with artificial potential field algorithm (ACOAPF) [27]: It is based on a distributed ACO algorithm with an improved transition rule without considering the range constraint, and the APF is introduced without considering the dynamic updating of the TPM.

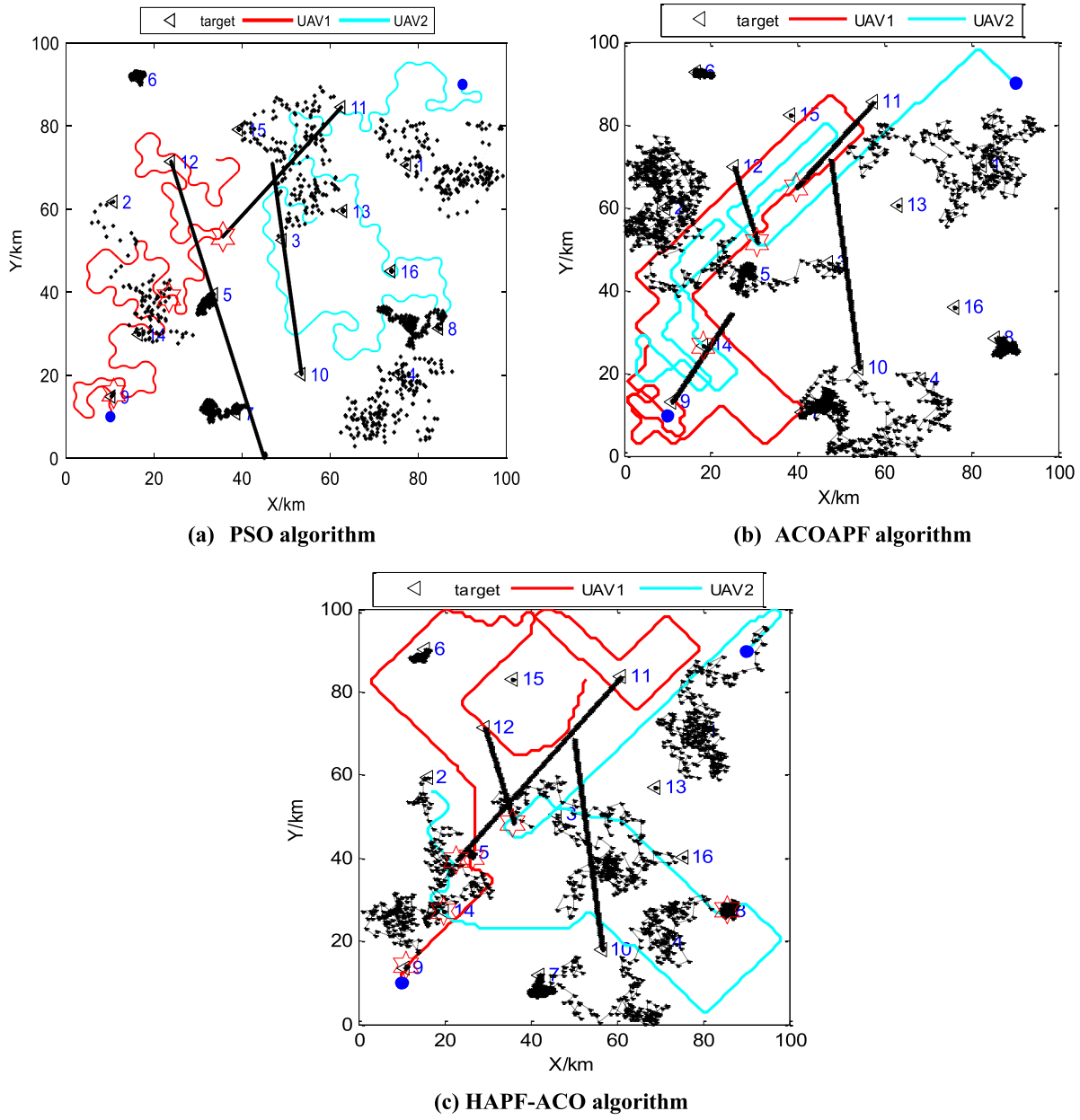

Fig. 3. Two UAVs' paths generated after 250 iterations for the mission with 16 targets.

Algorithm 3. A hybrid artificial potential field and ant colony optimization algorithm (HAPF-ACO): It is based on a distributed ACO algorithm with an improved transition rule considering the range constraint, and the APF is introduced considering the dynamic updating of the TPM.

The paths of the UAVs after 250 iterations obtained in the above three sets of experiments are shown in Fig. 3. The black triangles in the figure indicate the targets, the red hexagon stars indicate the destroyed targets, and the blue dots indicate the initial positions of the UAVs. As shown in Fig. 3(a), the UAV1 finds and attacks target 9, target 2 and target 11 under the PSO algorithm. As shown in Fig. 3(b), the UAV1 finds and attacks target 11, and UAV2 finds and attacks target 12 and target 14 under the ACOAPF algorithm. As shown in Fig. 3(c), after increasing the dynamic TPM, UAV1 under the HAPF-ACO algorithm discovers and attacks target 9 and target 5, and UAV2 discovers and attacks target 12, target 8, target 14 and target 11.

The mission area coverage rates and the numbers of destroyed targets under the three algorithms are shown in Fig. 4 and Fig. 5, respectively. The mission execution efficiency of the proposed HAPF-ACO algorithm is better than that of the PSO algorithm. In the early stage, the mission area coverage rates of the ACOAPF algorithm and HAPF-ACO algorithm are approximately the same, with the increase of the iterations, the advantage of the HAPF-ACO algorithm is more obvious. And as shown in Fig. 5, because of the introduction of the dynamic updating TPM, when there is a target near the UAV, it will quickly approach the target under the direct action of the potential field force, and the task execution efficiency is improved.

In addition, the simulations of three algorithms are carried out 30 times, and each algorithm's iteration number is 250. Two coverage metrics referred from [28] and the number of destroyed targets are used to evaluate the algorithms. The coverage rates of 250 iterations

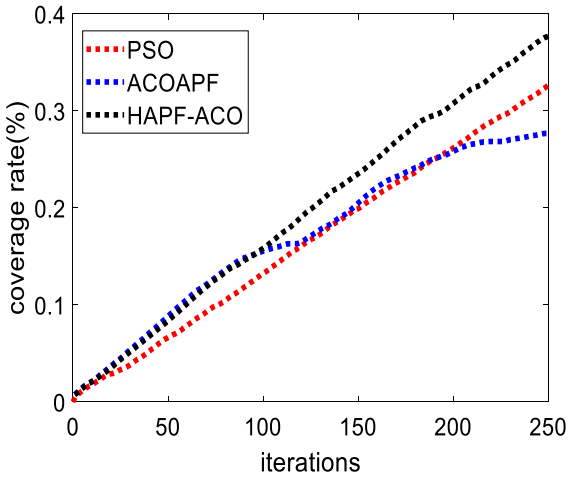

Fig. 4. Comparison on coverage rate of three algorithms.

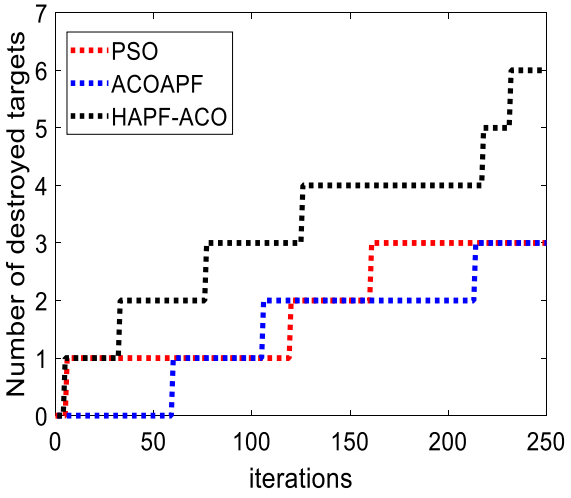

Fig. 5. Comparison on destroyed targets of three algorithms.

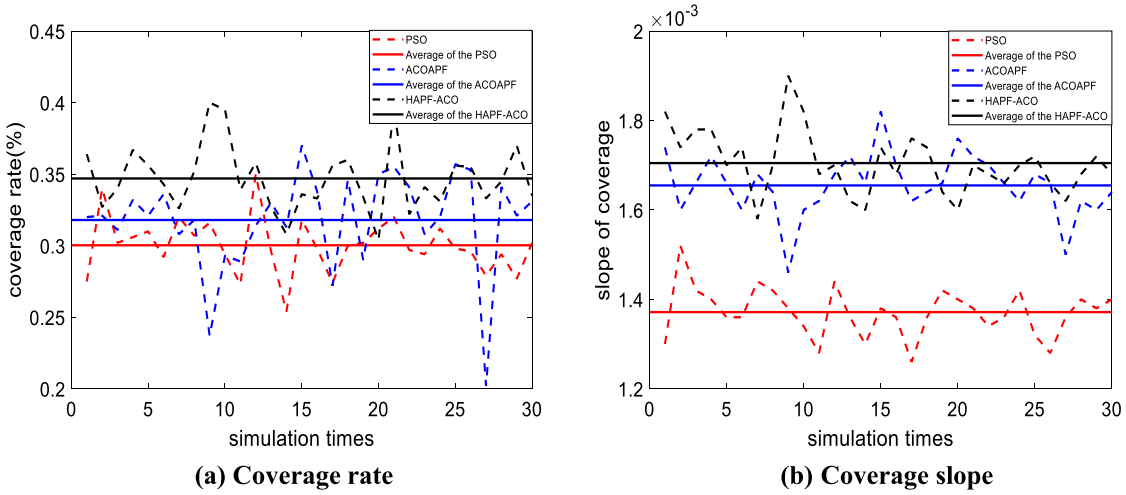

(a) Coverage rate **(b) Coverage slope**

Fig. 6. Comparisons on coverage metrics of three algorithms.

and the coverage slopes of first 50 iterations are shown in Fig. 6, while the numbers of destroyed targets are shown in Fig. 7, to exhibit the performance comparisons of three different algorithms. It is found that the UAVs under PSO algorithm can search and attack 2.5 targets and the UAVs under ACOAPF algorithm can search and attack 4.5 targets, while the UAVs under HAPF-ACO algorithm can search and attack 5.5 targets on average. Therefore, the average efficiency of the HAPF-ACO algorithm is much greater than that of the PSO and ACOAPF algorithms. Moreover, all the results show the statistically significant differences among three algorithms (with a p-value < 0.05) according to the Friedman's test. Therefore, the HAPF-ACO algorithm achieves the best performance than the other two algorithms.

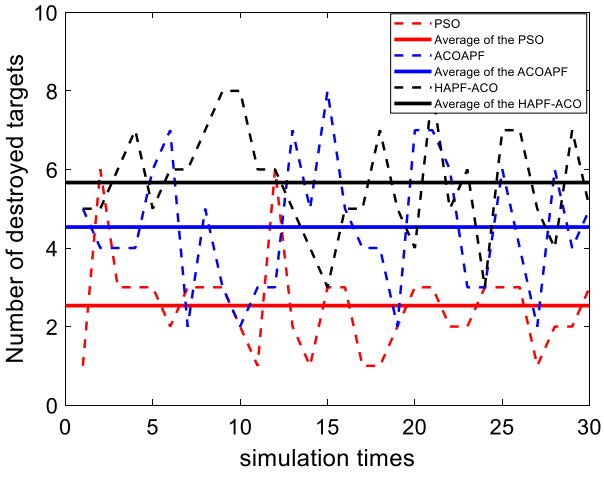

Fig. 7. Comparison on mission execution efficiency of three algorithms.

Table 3
Threat information.

Threat label	Coordinate (km)	Radius (km)
1	(5,40)	2
2	(30,85)	4
3	(63,30)	6
4	(30,15)	3
5	(70,85)	3

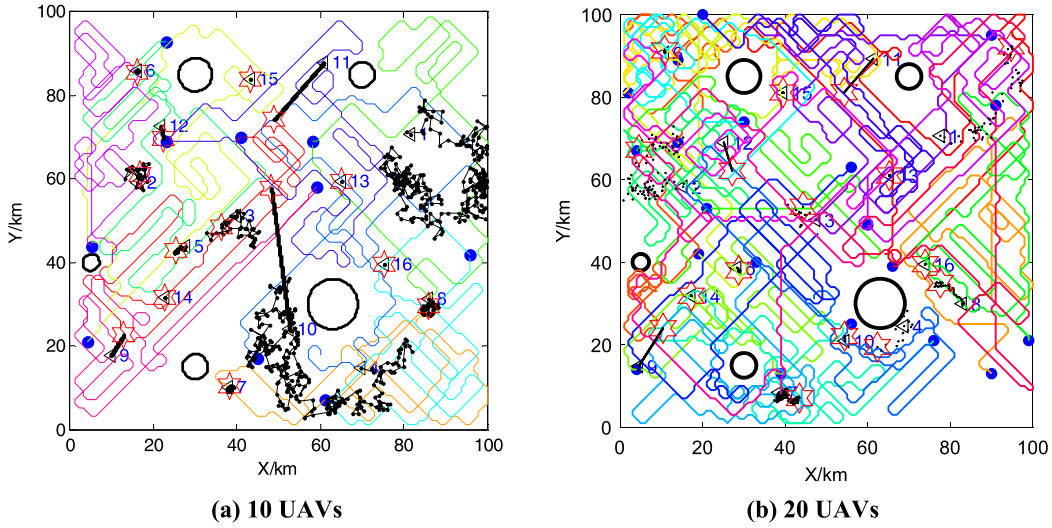

Fig. 8. Multiple UAVs' paths generated after 250 iterations with 5 threats.

4.3. Obstacle and collision avoidance performance analysis

Assuming that the swarm is composed of 10 UAVs and 20 UAVs respectively, in these two different cases, the initial positions and velocity directions of the UAVs are randomly generated. The maximum range of the UAV is 330 km. The expected number of neighbors $n_{topo} = 5$, the perceived radius of the UAV is 50 km. To verify the obstacle avoidance performance of the mission planning algorithm, 5 unknown threats are added in the above mission area. The threat information is shown in Table 3.

The UAV paths map after 250 iterations is shown in Fig. 8, where the black circles indicate the threat area. The mission area coverage rate and the number of destroyed targets are shown in Fig. 9 and Fig. 10, respectively. After 250 iterations, when the size of UAV swarm is 10, the coverage of the mission area reaches 84.5%, and the UAV swarm attacks 14 targets. It can be seen that the UAV swarm can effectively avoid the threat area while performing regional cooperative search-attack, and 7 UAVs have returned to the starting point under the range constraints, and the UAVs that have not returned to the starting point are also in the range of flight constraints. The simulation results show that the designed HAPF-ACO algorithm effectively realizes the online obstacle avoidance of UAV swarm by introducing the threat repulsion field.

However, when the size of UAV swarm is 20, the coverage of the mission area reaches 93.1%, and the UAV swarm attacks 16 targets. The coverage rates of 250 iterations and the coverage slopes of first 50 iterations are shown in Fig. 11. Although the coverage rate does not reach 100% due to the existence of obstacles and the range constraints, it can be found that the larger the UAV swarm's size is, the greater

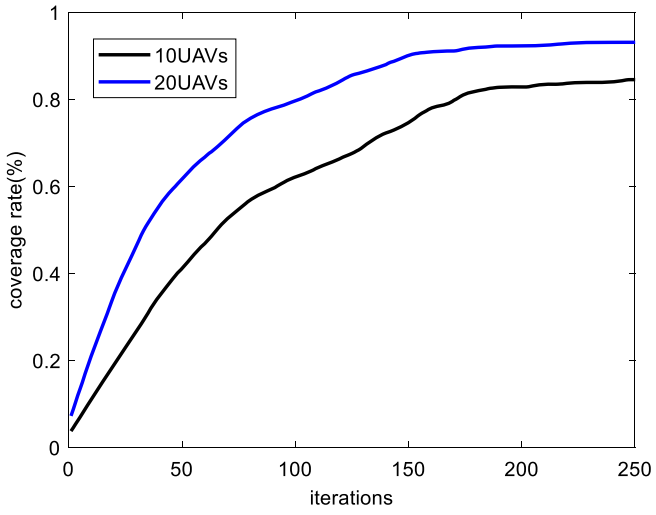

Fig. 9. Comparison on coverage rate for 10 UAVs and 20 UAVs with 5 threats.

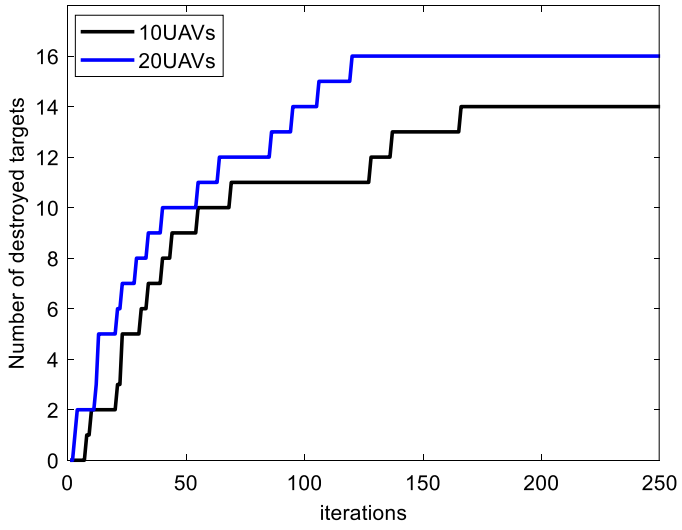

Fig. 10. Comparison on destroyed targets number for 10 UAVs and 20 UAVs with 5 threats.

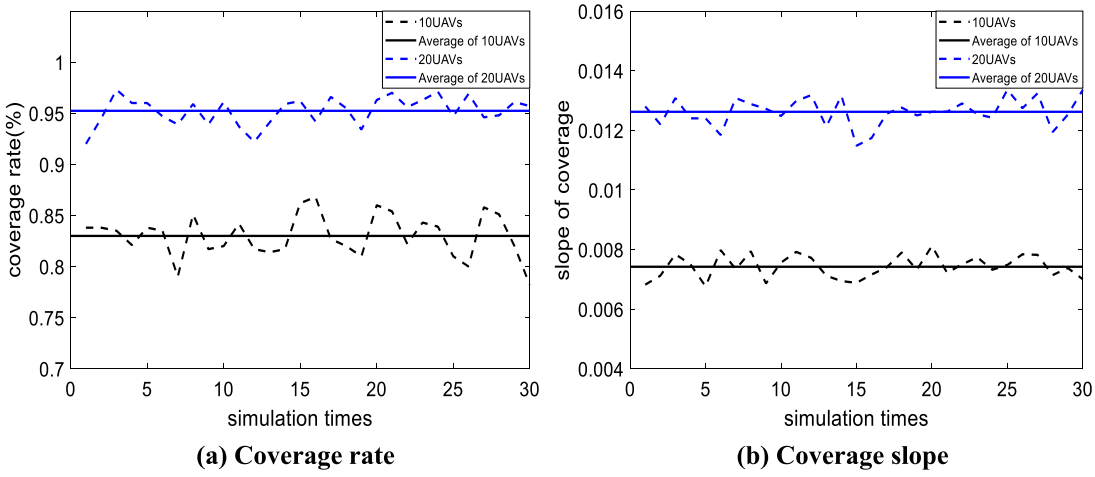

Fig. 11. Comparisons on coverage metrics for 10 UAVs and 20 UAVs with 5 threats.

the coverage efficiency is, each experiment is repeated 30 times to obtain statistically significant results. Furthermore, Fig. 12 shows that 20 UAVs can search and attack 15.7 targets on average, while 10 UAVs can search and attack 12.5 targets on average. Therefore, the higher number of UAVs can improve the mission execution speed.

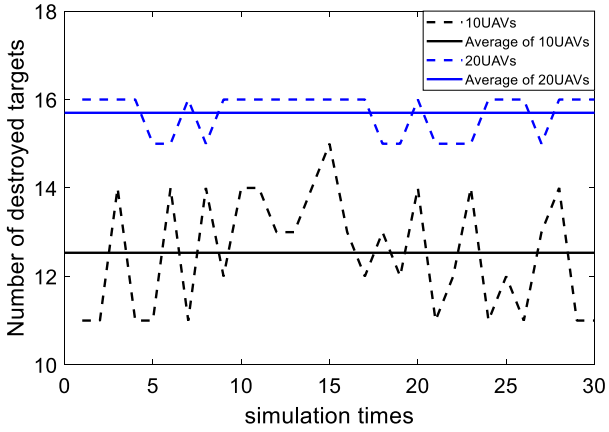

Fig. 12. Comparison on mission execution efficiency for 10 UAVs and 20 UAVs with 5 threats.

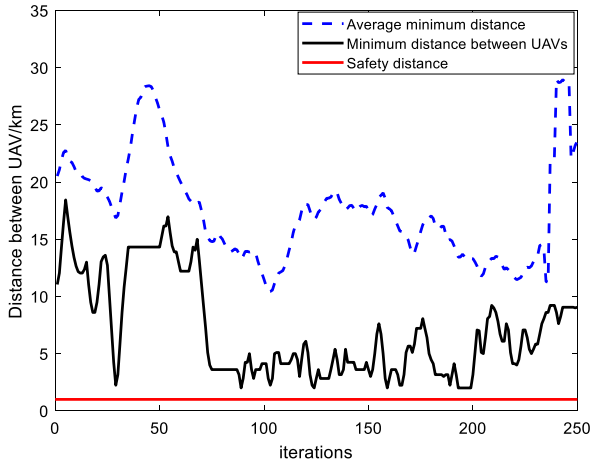

Fig. 13. Variation curves of average minimum distance, minimum distance and safety distance among 10 UAVs.

In addition, the minimum distance between UAVs during the search-attack is shown in Fig. 13, where the algorithm sets the safety distance between the UAVs $d_{\min} = 1$ km (1 grid). It can be seen that the minimum distance between UAVs is greater than the safety distance at any time. This is because when the distance between UAVs is too close, the UAV will be far away from neighbors with too close distance under the action of the designed repulsive field between the UAVs, thus ensuring the safety distance between the UAVs and realizing the online collision avoidance function of the swarm.

5. Conclusion

A novel intelligent cooperative mission planning algorithm abbreviated to HAPF-ACO is originally proposed, to solve the cooperative search-attack problem for UAV swarm. In this problem, four moving and time-sensitive target types are considered in the uncertain dynamic environment, and the constraints of maneuverability, collision avoidance, obstacle avoidance and flight range of UAV are considered. By constructing the TPM, the UAV can quickly approach the target near the UAV under the direct action of the APF, which mainly includes the target attraction field and threat repulsive field. A novel state transition rule is designed to ensure that the UAVs can return to the initial point or a specific destination within the maximum range.

Several simulations for studying the task execution efficiency and obstacle and collision avoidance performance are carried out. The results show that the proposed HAPF-ACO algorithm has highest execution efficiency compared with the PSO algorithm and ACOAPF algorithm, and realizes online obstacle avoidance and anti-collision of UAV swarm.

However, the cooperative search-attack problem in this study is aimed at the homogeneous UAVs. Therefore, the cooperation between heterogeneous UAVs (i.e., sensor difference, speed difference, attack difference) is more practical, which still needs to be studied in future work.

Declaration of competing interest

There is no conflicts of interest to this work.

References

[1] G. Danoy, M.R. Brust, P. Bouvry, Connectivity stability in autonomous multi-level UAV swarms for wide area monitoring, in: Proceedings of the Fifth ACM International Symposium on Development and Analysis of Intelligent Vehicular Networks and Applications, 2015, pp. 1–8.

[2] M. Mavrovouniotis, C. Li, S. Yang, A survey of swarm intelligence for dynamic optimization: algorithms and applications, Swarm Evol. Comput. 33 (2017) 1–17.
[3] M. Chen, F. Dai, H. Wang, DFM: a distributed flocking model for UAV swarm networks, IEEE Access 6 (2018) 69141–69150.
[4] Y.B. Wang, P. Bai, X.L. Liang, Reconnaissance mission conducted by UAV swarms based on distributed PSO path planning algorithms, IEEE Access 7 (2019) 105086–105099.
[5] C.F. Hu, Z.L. Zhang, N. Yang, H.S. Shin, Fuzzy multiobjective cooperative surveillance of multiple UAVs based on distributed predictive control for unknown ground moving target in urban environment, Aerosp. Sci. Technol. 84 (2019) 329–338.
[6] B. Shirani, M. Najafi, I. Izadi, Cooperative load transportation using multiple UAVs, Aerosp. Sci. Technol. 84 (2019) 158–169.
[7] P. Li, H.B. Duan, A potential game approach to multiple UAV cooperative search and surveillance, Aerosp. Sci. Technol. 68 (2017) 403–415.
[8] X.Y. Zhao, Q. Zong, B.L. Tian, Fast task allocation for heterogeneous unmanned aerial vehicles through reinforcement learning, Aerosp. Sci. Technol. 92 (2019) 588–594.
[9] W.R. Yao, N.M. Qi, N. Wan, Y.B. Liu, An iterative strategy for task assignment and path planning of distributed multiple unmanned aerial vehicles, Aerosp. Sci. Technol. 86 (2019) 455–464.
[10] W.N. Wu, X.G. Wang, N.G. Cui, Fast and coupled solution for cooperative mission planning of multiple heterogeneous unmanned aerial vehicles, Aerosp. Sci. Technol. 79 (2019) 131–144.
[11] M.M. Polycarpou, Y. Yang, K.M. Passino, A cooperative search framework for distributed agents, in: Proceedings of the 2001 IEEE International Symposium on Intelligent Control, Mexico City, Mexico, 2001, pp. 1–6.
[12] L.G. Pan, Q. Lu, X.G. Xie, A probability distribution based cooperative search approach for stochastic source localization, in: 27th International Symposium on Industrial Electronics, IEEE, Cairns, QLD, Australia, 2018, pp. 585–590.
[13] L.F. Bertuccelli, J.P. How, Search for dynamic targets with uncertain probability maps, in: American Control Conference, IEEE, Minneapolis, MN, USA, 2006.
[14] T. Millet, D. Casbeer, T. Mercker, J. Bishop, Multi-agent decentralized search of a probability map with communication constraints, in: AIAA Guidance, Navigation and Control Conference, 2013.
[15] M. Paradzik, G. Ince, Multi-agent search strategy based on digital pheromones for UAVs, in: 24th Signal Processing and Communication Application Conference, IEEE, Zonguldak, 2016, pp. 233–236.
[16] F. Yang, Cooperative search of UAV swarm based on improved ant colony algorithm in uncertain environment, in: Proceedings of 2017 IEEE International Conference on Unmanned Systems, Beijing, 2017, pp. 231–236.
[17] C. Erignac, An exhaustive swarming search strategy based on distributed pheromone maps, in: Proceedings of AIAA Infotech@Aerospace 2007 Conference and Exhibit, AIAA, California, 2007, pp. 1–16.
[18] X. Xiao, Z. Dong, J. Wu, A cooperative approach to multiple UAVs searching for moving targets based on a hybrid of virtual force and receding horizon, in: 10th International Conference on Industrial Informatics, IEEE, Beijing, 2012, pp. 1228–1233.
[19] R. Wang, B. Xiao, L. Ru, Cooperative search approach for UAVs via pigeon-inspired optimization and Markov moving targets, in: 2018 Chinese Automation Congress, IEEE, Xi'an, China, 2018, pp. 2007–2012.
[20] X.H. Wang, Y.M. Deng, H.B. Duan, Edge-based target detection for unmanned aerial vehicles using competitive bird swarm algorithm, Aerosp. Sci. Technol. 78 (2018) 708–720.
[21] B.M. Jeong, J.S. Ha, H.L. Choi, MDP-Based Mission Planning for Multi-UAV Persistent Surveillance, 2014 14th International Conference on Control, Automation and Systems (ICCAS), IEEE, Korea, October 22–25, 2014.
[22] I.C. Price, G.B. Lamont, GA directed self-organized search and attack UAV swarms, in: Proceedings of the 2006 Winter Simulation Conference, IEEE, Monterey, CA, 2006, pp. 1307–1315.
[23] C. Gao, Z.Y. Zhen, H.J. Gong, A self-organized search and attack algorithm for multiple unmanned aerial vehicles, Aerosp. Sci. Technol. 54 (2016) 229–240.
[24] Z. Zhen, D. Xing, C. Gao, Cooperative search-attack mission planning for multi-UAV based on intelligent self-organized algorithm, Aerosp. Sci. Technol. 76 (2018) 402–411.
[25] F. Yan, X.P. Zhu, Z. Zhou, Y. Tang, Heterogeneous multi-unmanned aerial vehicle task planning: simultaneous attacks on targets using the Pythagorean hodograph curve, Proc. Inst. Mech. Eng., G J. Aerosp. Eng. 233 (13) (2019) 4735–4749.
[26] A.G. Shem, T.A. Mazzuchi, S. Sarkani, Addressing uncertainty in UAV navigation decision-making, IEEE Trans. Aerosp. Electron. Syst. 44 (1) (2008) 295–313.
[27] X. Tan, D.F. Chen, A hybrid approach of path planning for mobile robots based on the combination of ACO and APF algorithms, in: International Workshop on Intelligent Systems and Applications, IEEE, Wuhan, China, 2009.
[28] M. Rosalie, M.R. Brust, G. Danoy, S. Chaumette, P. Bouvry, Coverage optimization with connectivity preservation for UAV swarms applying chaotic dynamics, in: 2017 IEEE International Conference on Autonomic Computing, Columbus, OH, USA, 2017, pp. 113–118.